Published in final edited form as:

Ultrasound Med Biol. 2018 May ; 44(5): 1012–1021. doi:10.1016/j.ultrasmedbio.2017.11.006.

Pulmonary Capillary Hemorrhage Induced by Different Imaging Modes of Diagnostic Ultrasound

Douglas L. Miller[1], **Zhihong Dong**[1], **Chunyan Dou**[1], and **Krishnan Raghavendran**[2]

[1]Department of Radiology, University of Michigan Health System, Ann Arbor MI 48109

[2]Department of Surgery, University of Michigan Health System, Ann Arbor MI 48109

Abstract

The induction of pulmonary capillary hemorrhage (PCH) is a well-established nonthermal biological effect of pulsed ultrasound in animal models. Typically, research has been done using laboratory pulsed ultrasound systems with a fixed beam, and recently by B mode diagnostic ultrasound (DUS). In this study, a GE Vivid 7 Dimension ultrasound machine with 10L linear array probe was used at 6.6 MHz to explore the relative PCH efficacy of B mode imaging, M mode (fixed beam), Color Angio mode Doppler imaging, and pulsed Doppler mode (fixed beam). Anesthetized rats were scanned in a warmed water bath and thresholds were determined by scanning at different power steps, 2 dB apart, in different groups of 6 rats. Exposures were performed for 5 min, except for a 15 s M mode group. Peak rarefactional pressure amplitude thresholds were 1.5 MPa for B mode and 1.1 MPa for Angio Doppler mode. For the non-scanned modes, thresholds were 1.1 MPa for M mode and 0.6 MPa for pulsed Doppler mode with its relatively high duty cycle ($7.7{\cdot}10^{-3}$ versus $0.27{\cdot}10^{-3}$ for M mode). Reducing the duration of M mode to 15 s (from 300 s) did not significantly reduce PCH (area, volume or depth) for some power settings, but the threshold was increased to 1.4 MPa. Pulmonary sonographers should be aware of this unique adverse bioeffect of diagnostic ultrasound, and should consider reduced on screen Mechanical Index settings for potentially vulnerable patients.

Keywords

Pulmonary ultrasound; comet tail artifact; bioeffects of ultrasound; ultrasound dosimetry; diagnostic ultrasound safety

Introduction

The induction of pulmonary capillary hemorrhage (PCH) is a well-established non-thermal biological effect of pulsed ultrasound in animal models first reported in 1990 (Child et al. 1990). We have recently studied PCH induction by B mode diagnostic ultrasound (Miller,

Corresponding author: Douglas L. Miller, 3240A Medical Sciences Building I, University of Michigan Health System, 1301 Catherine Street, Ann Arbor MI 48109-5667, Tel: (734) 647-3344, FAX: (734) 764-8541, douglm@umich.edu.

2012). This phenomenon appears to be the only clearly demonstrable bioeffect of diagnostic ultrasound reported to occur in mammals (in the absence of ultrasound contrast agents). The safety issue presented by PCH initially was considered to be of low risk, because only incidental lung exposure was expected (Church et al. 2008). However, in recent years, direct pulmonary examination by diagnostic ultrasound has become routine in point-of-care ultrasound and other settings.

Experimental use of pulmonary diagnostic ultrasound (PDUS) was explored as early as 1967 for detection of pleural effusion (Joyner et al. 1967) and pulmonary embolism (Miller et al. 1967). Probably the first routine use of PDUS was to rule out pneumothorax using modern PDUS (Lichtenstein and Menu, 1995). PDUS has been found to be valuable in diagnosis of pneumonia, pulmonary edema, embolism, atelectasis, diffuse parenchymal disease, respiratory distress syndrome, and lung cancer (Sartori and Tombesi, 2010). Chest sonography is accepted in children for diagnosis of neonatal respiratory distress syndrome (Copetti et al. 2008) and pneumonia (Liu et al. 2014; Pereda et al. 2015). The rapidly expanding use of portable ultrasound machines allows PDUS to be performed by the physician at the bedside, not unlike the ubiquitous stethoscope (Lumb and Karakitsos 2015; Irwin and Cook, 2016; Sekiguchi, 2016). Point-of-care PDUS has become routine in intensive care, emergency care and other medical settings (Volpicelli, 2013; Lichtenstein, 2014; Ahmad and Eisen, 2015; Dietrich et al. 2017). There are now at least 10 different diagnostic signs for lung ultrasound (Lichtenstein, 2015). PDUS can involve 8 or more scan zones of the antero-lateral and posterior chest (Gargani and Volpicelli, 2014). Extensive scanning for quantitative analysis of PDUS comet tail artifacts (CTAs) aids in characterization of high altitude pulmonary edema (Fagenholz et al. 2007), chest congestion in dialysis patients (Zoccali et al. 2013; Weitzel et al. 2015), and other conditions (Dietrich et al. 2016). The total usage of PDUS is impossible to determine because point-of-care ultrasound is performed in so many settings, often informally without billing records and often routinely on a daily basis to follow patient progress (Hall et al, 2016; Sferrazza Papa et al. 2017). Thus, the safety issue has become worrisome: it is possible that vulnerable patients are unknowingly injured by PDUS.

Ultrasound induced PCH has received significant interest due to the apparent safety issue (AIUM, 2000; Church et al. 2008). Typically, research has been performed using laboratory pulsed ultrasound systems, or recently using the B-mode of DUS. In our recent study, the laboratory pulsed ultrasound had somewhat lower thresholds than B mode ultrasound (Miller et al. 2015a), which might be expected because it is focused at one position, while B mode delivers a much lower number of pulses to a specific point when the beam scans the lung surface. Thresholds have been sought for different conditions and parameters, but the number of parameters, in situ values of exposure, and possible patient conditions complicate this process. For example, the PCH threshold has little dependence on ultrasound frequency (Miller et al. 2015b), which makes use of the on screen Mechanical Index ($\boldsymbol{MI_{OS}}$) problematical for simple safety adjustments. The thresholds also depend on biological conditions such as age (Dalecki et al. 1997; O'Brien et al. 2003), specific anesthetics (Miller et al. 2015c) and even common patient sedatives (Miller et al. 2016a). More definitive information on the etiology of PCH would be valuable to clarify the extensive data-base

presently available and to assist in mitigating risks. M mode is commonly used for pulmonary examinations, with the ultrasound sea-shore sign indicating normal lung function (Ahmad and Eisen, 2015). Other modes can also interact with the lung during transthoracic examination, such as pulsed Doppler and Color Doppler imaging in echocardiography for pulmonary hypertension (Bossone et al. 2015; Vargas and Lopez-Candales, 2016). The purpose of the present study was to detail PCH occurrence and thresholds in a rat model of PDUS for B mode, M mode, pulsed Doppler and Color Angio mode Doppler imaging.

Methods

Ultrasound

A clinical GE Vivid 7 Dimension (GE Vingmed Ultrasound AS, Horten, Norway) diagnostic ultrasound machine was used in this study. The 10L linear array probe was used throughout. The image application was set up with 3 cm depth and single focus at 1.3 cm image depth. The −6dB width of the beam was 1.2 mm. The machine was operated in four standard modes: B mode, M mode, Pulsed Doppler mode, and color Doppler Angio mode, as listed in Table 1 (together with PCH thresholds, see Results). The frequency was set to 7.5 MHz for B and M mode, 6.6 MHz for pulsed Doppler and 6.4 MHz for Angio mode. The probe was held with a gimbal mount in a heated water bath filled with vacuum degassed water. The ultrasound pulse parameters were measured at the positon of the maximum PRPA (1.3 cm depth on the probe axis) using a calibrated hydrophone with a 0.2 mm sensitive spot (model HMA-0200, Onda Corp., Sunnyvale, CA) and are listed in Table 1. The digitized pulse pressure waveform, measured in water, was derated by an attenuation factor of 1.2 dB/cm-MHz (Miller et al. 2015b), which was −4 dB for the approximate chest wall thickness of 0.5 cm, and ultrasound frequency of 6.6 MHz. This provided the approximate in situ values at the lung surface of the peak rarefactional pressure amplitude (PRPA), peak compressional pressure amplitude and peak mean pressure amplitude (PMPA). The pulse duration was calculated as 1.25 times the interval between the 10% and 90% time points of the instantaneous pulse intensity, and the spatial peak pulse average intensity ($\boldsymbol{I_{SPPA}}$). was also calculated as the average of the instantaneous pulse intensity over the pulse duration. The observed center frequencies for all the modes were approximately 6.6 MHz. The PRPA is the primary exposure parameter, because it is used in the on screen Mechanical Index (the regulated parameter for nonthermal risks). The physical mechanism for PCH is uncertain, but appears to depend on the peak compressional pressure amplitude as well as the PRPA (Baily et al. 1996; Frizzel et al. 2003), or specifically on the $\boldsymbol{I_{SPPA}}$ (Miller, 2016). The PMPA and $\boldsymbol{I_{SPPA}}$ were also determined and specified here.

For assessment of the exposure–response, the parameters were measured for power settings −2 dB apart, with the maximum of 0 dB on the ultrasound machine. In situ Mechanical Index ($\boldsymbol{MI_{IS}}$) values were computed by dividing the peak rarefactional pressure amplitude by the square root of 6.6 MHz. The on-screen values were $\boldsymbol{MI_{OS}}$ = 1.2 for B, M and Angio mode, and $\boldsymbol{MI_{OS}}$ = 0.4 for pulsed Doppler, which were comparable to the calculated in situ values. Examples of pulses from each mode are shown in Figure 1, together with the sequence of pulses over a span of 2 to 9 ms received by the hydrophone from the fixed beam for M mode or pulsed Doppler mode, or during an imaging sweep for B mode or Angio

Doppler mode (typically, no, or very low pulses are received between the scan sweeps). For the Angio Doppler mode the exposure was somewhat confused by the associated B mode scan in duplex ultrasound, which provided a grey scale background image for the low resolution Angio Doppler color image. The pulse sequences illustrate the differences in the numbers of higher amplitude pulses impinging on a point of the lung surface for each mode. For example, B mode at 60 fps delivered 60 of the maximal pulses (see Fig. 1) per second, while M mode delivered 1,000 of the maximal pulses per second.

Animal preparation

All *in vivo* animal procedures were conducted with the approval and guidance of the Institutional Animal Care and Use Committee, University of Michigan, Ann Arbor, MI. Female Sprague Dawley rats (Charles River, Wilmington, MA, USA) were used for this research. The rats weighed an average of 240 ± 18 gm and each was anesthetized with IP injection of 91 mg/kg ketamine (Zetamine™ ketamine hydrochloride injection, MWI, Boise, ID, USA) plus 9 mg/kg IP xylazine (XylaMed™ xylazine injection, MWI, Boise, ID, USA). This anesthesia combination has been used for most research on ultrasound induced PCH. These methods duplicate the methods of the previous study of the frequency dependence of PCH thresholds (Miller et al. 2015b).

The right thorax of each rat was shaved and depilated for ultrasound transmission. For exposure, the rats were mounted on a plastic board and aligned vertically in the 38 °C water bath. The water bath setup allowed precise aiming of the exposure probe, and maintained the body temperature of the anesthetized rats. The scan plane was aimed between the ribs to obtain a clear bright-line lung surface image at 1.2 to1.3 cm image depth at the medial lobe. The 7.5 MHz B mode was set at −20 dB power (pressure amplitudes reduced by a factor of ~10) for aiming to avoid potential lung injury during the aiming procedure. A pulse oximeter probe (SurgiVet V3395 TPR, Smiths Medical Inc. St Paul, MN USA) was placed briefly on a hind paw after anesthesia to check the heart rate and percent oxygen saturation (%SPO_2), which averaged 272 ± 28 beats per min and 79 ± 6 %, respectively.

After aiming, the desired mode was started from a saved application created for this study, the power was quickly raised to the desired setting, and timed for 5 min, after which the power was quickly lowered to −20 dB. Groups of 6 rats each were scanned using one of 6 scan mode protocols, at a specific power setting, as listed in Table 2. The sham condition simply kept the −20 dB aim-setting on for 5 min to demonstrate lack of effect. One exposure condition with M mode was timed manually to about 15 s (rather than 5 min), which accommodated the horizontal M mode display sweep time of 16 s (the longest available). For M mode the vertical indicator line in the B mode image was aimed at the center of the bright-line lung image, and then the B mode was frozen. Images were saved before and after each exposure. For pulsed Doppler, the indicator line in the B mode image was aligned vertically, as for M mode, with the sample volume set at the lung surface.

The images provide information about the PCH effect by displaying “B-lines”, which are comet tail artifacts (CTAs) that project inward perpendicular to the lung surface image. These do not quantify the hemorrhage depth, but do give a qualitative indication, which increases with time as the exposure progresses. The width of the bright-line lung surface

image was measured, together with the width which was involved with the CTAs. The percentage width of CTAs was calculated as one measure of the PCH effect.

Five min after exposure, each rat was sacrificed under anesthesia by exsanguination of the inferior vena cava. The trachea was occluded to maintain lung volume and the heart and lungs were removed together. The right lobes, which were the target of the imaging, were then examined and photographed using a stereomicroscope with digital camera (Spot Flex, Diagnostic Instruments Inc., Sterling Heights, MI USA). The photographs of the lungs were used to measure the approximate diameter and area of the region of PCH on the lung surface using image analysis software (Spot v. 5.1, Diagnostic Instruments, Inc., Sterling Heights, MI USA). The area measurement involved freehand outlining of the PCH regions on each lung to include irregularities in the shape of the PCH area. PCH depth was measured in fixed samples as described previously (Miller et al. 2016b). Briefly, the lungs were fixed by immersion in 4% buffered formaldehyde and suspended from a tether in an upside down 50 ml tube. When fully fixed (> 1 week) the lungs were switched to 70 % ethanol for examination of the PCH volume. The PCH region was cut into about 2 mm thick slabs to measure the depth of the hemorrhage, and one slab was used for histology as a means to confirm the depth, as described previously (Miller et al. 2016b). The PCH volume was calculated approximately as the observed fresh PCH area on the surface times the average measured depth for fixed tissue. The depth measurement was less certain than the fresh measurements due to unavoidable distortion and discoloration during fixation. The thickness of the lung lobe (3.5 mm ± 1.4 mm) was approached by the depth of PCH in only a few samples for the higher power settings.

Experimental Plan and Statistics

For each exposure condition, rats groups (n=6, except 7 for 15 s M mode at 0 dB, and 8 for Pulsed Doppler at −4 dB) were exposed at different power settings. The lowest power setting for each mode was determined by gauging the setting with no significant PCH. In all, 26 groups were completed, see Table 2. Exposures were conducted on a given day for the groups of a single exposure condition (rather than randomly for all groups) to provide consistent exposure-response data. Statistical analysis was performed using SigmaPlot for Windows V. 11.0 (Systat Software Inc., San Jose CA, USA). The Mann-Whitney Rank Sum test was used to compare means of measured PCH area between exposure groups and shams, and the t-test was used for other comparisons. Statistical significance was assumed at $p<0.05$. A threshold for each exposure group was determined by linear regression of all data points with observed PCH as the zero PCH intercept PRPA. This was also approximately equal to the mean of the lowest exposure with a statistically significant PCH area (occurrence of 5/6) and the next lower setting, however the regression method had the advantage of taking into account all the data points with any PCH.

Results

The B mode exposure results were similar to previous studies (Miller, 2012; Miller et al. 2016b), except for the use of the 10L linear array probe. An example of the images and resulting PCH is shown in Fig. 2. The initial image shows the typical bright-line lung surface

image at 1.3 cm depth, with artifactual images appearing below the line, including an A line at about 2.6 cm. After 5 min of scanning the image shows extensive artifactual CTAs (B lines) extending from the lung surface reflection into the lung. A gap in the CTAs was caused by a rib shadow. The resulting PCH cuts across the medial lobe, with a spot also on the caudal lobe. The data on CTAs, PCH area on the lung surface, hemorrhage volume and depth are presented in Table 2, and the exposure-response trend with linear regression is illustrated in Fig. 3. The CTAs are reliably predictive of the occurrence and length of PCH across the lung surface. For the lower power settings, the PCH effect becomes hit-or-miss, and a proportion of exposed rats fail to show any PCH. The proportion of positive results is also listed in Table 2. By the Z test of proportions, including the Yates correction for relatively small n, the p values for 6/6, 5/6, and 4/6 were 0.004, 0.019 and 0.066, respectively. The 4/6 and all lesser proportions are not statistically significant (although it should be noted that the effect was seen in some of the rats even though the occurrence as not significant as a group, and this was included in the linear regression threshold determination). The p values are also given, as calculated for the Mann Whitney Rank Sum test for PCH area for exposed relative to sham. The thresholds are listed in Table 1 for the PRPA, PMPA, $\boldsymbol{I_{SPPA}}$ and in situ $\boldsymbol{MI_{IS}}$.

An example of the images and resulting PCH for a 15 s M mode exposure is shown in Fig. 4. The PCH appeared in the M-mode trace as a progressive noisy obscuration by CTAs of the normal sub-pleural artifacts, such as the A line. Measured results and thresholds are given in Tables 1 and 2. For M mode, the PCH was a spot on the lung surface, smaller than the PCH for the scanned beam, with a single narrow CTA region in the ultrasound image. The exposure-response trend with linear regression is plotted in Figure 5. The results for the 5 min and 15 s M mode exposures at 0 dB and −2 dB were not significantly different, with p=0.08 and 0.11, respectively. However, these protocols produced statistically significantly different results for −4 dB (p=0.013) and −6 dB (p=0.039), with a lower threshold for the 5 min duration (Table 1). The depth of hemorrhage produced by the M mode was not greatly deeper for the 5 min than for the 15 s exposure protocol, with no significant difference at 0 dB (p=0.18), and virtually identical results at −2 and −4 dB.

An example of the images and resulting PCH for the Angio Doppler mode exposure is shown in Fig. 6. The image showed some Doppler signal artifacts below the lung surface, in addition to the CTAs in the B mode background image. The color Doppler images were variable during exposure, possibly indicative of the changes in gas configuration and content as PCH fills alveoli. The results for PCH area are plotted in Fig. 3 for comparison to the B mode image results. In Table 2, the results are comparable, although the Angio Doppler mode had a slightly lower threshold for PCH.

An example of the before-and-after B mode images and resulting PCH for the pulsed Doppler mode exposure are shown in Fig. 7. The B mode image showed clear CTAs after exposure, similar to the M mode result. The results for PCH area are plotted in Fig. 5 for comparison to the M mode image results. The pulsed Doppler mode had significant PCH at the 0 and −2 dB power settings (Table 2), and the PCH area (p=0.43), volume (p=0.33) and maximum depth (p=0.43) were not significantly different from the M mode at the −2 dB setting. However, the ultrasound parameters of this setting were much lower ($\boldsymbol{I_{SPPA}}$ = 27 W

cm^{-2}), than for the M mode ($\boldsymbol{I_{SPPA}}$ = 321 W cm^{-2}). The PCH threshold for pulsed Doppler mode was the lowest of all the exposure modes (Table 1).

Discussion

PCH thresholds were detailed in our rat model of PDUS using a standard diagnostic ultrasound system. Previous research on PCH has utilized laboratory exposure systems (Church et al. 2008) or more recently, B mode diagnostic ultrasound (Miller, 2012; Miller et al. 2015b). A 38 mm wide 10L probe was used in this study at 6.6 MHz (observed) for B mode and the other important diagnostic ultrasound modes, including M mode, pulsed Doppler and Doppler Angio mode (also called power Doppler) imaging. M mode is commonly used for pulmonary examinations, and Doppler modes can also interact with the lung during transthoracic echocardiographic examination, such as for pulmonary hypertension. Exposures were performed for 5 min, except for a 15 s M mode protocol, for a range of power settings −2 dB apart, in different groups of rats. Ultrasound parameters for the 0 dB setting are listed in Table 1, and the pulse waveforms are illustrated in Figure 1 for the lowest setting with statistically significant PCH area induction. The on screen Mechanical Index was limited to $\boldsymbol{MI_{OS}}$ = 1.2 for our machine, and it should be noted that the general guideline upper limit for diagnostic ultrasound is 1.9 (potentially 1.6 times higher PRPA and about 2.5 times higher power or intensity). Images and PCH on the lung surface are presented in Figures 2, 4, 6 and 7 for B mode, M mode, Angio Doppler mode, and pulsed Doppler modes, respectively. Detailed endpoint results are listed in Table 2 and displayed in Fig. 3 (B and Angio modes) and Fig. 5 (M and pulsed Doppler modes). I_{SPPA} thresholds (Table 1) for M and Angio Doppler modes (50 and 42 W cm^{-2}) were somewhat less than for B mode (87 W cm^{-2}), but the pulsed Doppler threshold was much less (12 W cm^{-2}). The B mode threshold result (1.5 MPa) was somewhat higher than in a previous study with a 4.5 MHz B mode threshold of 1.28 MPa (Miller et al. 2015b) using a different probe. The greater efficacy of the pulse Doppler mode may be due to its continuous delivery of relatively long pulses (1130 ns) at a relatively short pulse repetition period (0.147 ms), which is in accord with the earliest observations of PCH variation with pulse duration (Child et al. 1990; O'Brien et al. 2003). Here, the duty cycle (fractional on-time) was $0.27{\cdot}10^{-3}$ for the M mode but $7.7{\cdot}10^{-3}$ for the pulsed Doppler mode, a factor of 28.5 greater, which likely explains the greater efficacy.

The exposure duration of 5 min was used to find the lowest thresholds (worst case), but reducing the duration of M mode exposures to 15 s (from 300 s) did not significantly reduce PCH (area, volume or depth) for some power settings. The threshold was however increased from 1.1 to 1.4 MPa. In terms of the in situ $\boldsymbol{MI_{IS}}$, thresholds were $\boldsymbol{MI_{IS}}$ = 0.24 for pulsed Doppler, $\boldsymbol{MI_{IS}}$ = 0.58 for B mode and $\boldsymbol{MI_{IS}}$ = 0.54 for 15 s M mode. The 15 s threshold of 1.4 MPa PRPA was less than a threshold of 2.8 MPa reported by Zachary et al. (2001). The ultrasound parameters for the laboratory system were 5.6 MHz, 1,140 ns pulse duration, 1 kHz PRF, 10 s exposure duration and 0.466 mm beam diameter (Zachary et al. 2001). In this present work, M mode parameters were 6.6 MHz, 269 ns pulse duration, 1 kHz PRF, 15 s exposure duration and 1.150 mm beam diameter. This difference was attributed previously to a longer exposure duration (Miller et al. 2015a), but here the exposure duration was similar. Possibly the greater beam diameter and 15 s duration yielded greater sensitivity in this study.

A related study at 2.8 MHz with pulse durations of up to 11,600 ns (1 KHz PRF, 10 s exposure duration) gave a threshold of about 2 MPa (O'Brien et al. 2003b).

PCH has unique clinical significance as the only known risk for adverse bio-effects for (non-contrast) diagnostic ultrasound. PCH involves breaching of the alveolar-capillary interface and therefore should be considered to be a pathologically significant finding. Due to a complex dependence not only on ultrasound parameters but also on patient conditions, the potential patient risk is uncertain. Likewise the medical the significance of PCH injury in the much larger human lung is also uncertain. However, pulmonary diagnostic ultrasound can and should be performed without risk of any adverse bioeffects. The 15 s M mode result indicates that reducing examination duration might not be very effective in reducing risk (i.e., hurrying an exam to finish in half the time might not be a wise strategy for risk reduction). Simply reducing power (or on screen $\boldsymbol{MI_{os}}$) may be a better strategy for at risk patients. Use of $\boldsymbol{MI_{os}}$ less than 0.4 appears to eliminate the risk of the occurrence of PCH (Church et al. 2008; AIUM 2015), with the possible exception of pulsed Doppler ultrasound (Table 1) which is not typically used for direct lung studies. The use of $\boldsymbol{MI_{os}} < 0.4$ may, however, not provide adequate images in some patients, for which the actual lung surface exposure would be substantially less than expected from the $\boldsymbol{MI_{os}}$ value (e. g. with thick chest wall). Further work is needed to provide science-based advice on the optimal application of pulmonary ultrasound for all patients.

Conclusions

Pulmonary capillary hemorrhage was observed in rats for B mode, M mode, Angio Doppler mode and pulsed Doppler mode using a typical clinical diagnostic ultrasound machine. M mode and Angio Doppler mode were more deleterious than B mode, and pulsed Doppler mode resulted in the largest PCH. Pulmonary sonographers should be aware of this possible adverse bioeffect, and the possible use of lower $\boldsymbol{MI_{os}}$ settings for risk reduction in potentially vulnerable patients.

Acknowledgments

This study was supported by the National Heart Lung and Blood Institute via grant number HL116434. The information contained herein does not necessarily reflect the position or policy of the US government, and no official endorsement should be inferred.

References

Ahmad, S., Eisen, LA. Lung ultrasound: the basics. In: Lumb, P., Karakitsos, D., editors. Critical care ultrasound. Vol. Ch 19. Philadelphia: Elsevier; 2015. p. 106-110.

American Institute of Ultrasound in Medicine [no authors listed]. Section 4--bioeffects in tissues with gas bodies. J Ultrasound Med. 2000; 19:97–108. 154–68. [PubMed: 10680616]

American Institute of Ultrasound in Medicine. Statement on Mammalian Biological Effects in Tissues with Naturally Occurring Gas Bodies. 2015. http://www.aium.org/resources/statements.aspx

Bailey MR, Dalecki D, Child SZ, Raeman CH, Penney DP, Blackstock DT, Carstensen EL. Bioeffects of positive and negative acoustic pressures in vivo. J Acoust Soc Am. 1996; 100:3941–3946. [PubMed: 8969491]

Bossone E, Ferrara F, Grünig E. Echocardiography in pulmonary hypertension. Curr Opin Cardiol. 2015; 30:574–86. [PubMed: 26447500]

Child SZ, Hart man CL, Schery LA, Carstensen EL. Lung damage from exposure to pulsed ultrasound. Ultrasound Med Biol. 1990; 16:817–25. [PubMed: 2095012]

Church CC, Carstensen EL, Nyborg WL, Carson PL, Frizzell LA, Bailey MR. The risk of exposure to diagnostic ultrasound in postnatal subjects: nonthermal mechanisms. J Ultrasound Med. 2008; 27:565–92. [PubMed: 18359909]

Copetti R, Cattarossi L, Macagno F, Violino M, Furlan R. Lung ultrasound in respiratory distress syndrome: a useful tool for early diagnosis. Neonatology. 2008; 94:52–59. [PubMed: 18196931]

Dalecki D, Child SZ, Raeman CH, Cox C, Penney DP, Carstensen EL. Age dependence of ultrasonically induced lung hemorrhage in mice. Ultrasound Med Biol. 1997; 23:767–776. [PubMed: 9253825]

Dietrich CF, Mathis G, Blaivas M, Volpicelli G, Seibel A, Wastl D, Atkinson NS, Cui XW, Fan M, Yi D. Lung B-line artefacts and their use. J Thorac Dis. 2016; 8:1356–1365. [PubMed: 27293860]

Dietrich CF, Goudie A, Chiorean L, Cui XW, Gilja OH, Dong Y, Abramowicz JS, Vinayak S, Westerway SC, Nolsøe CP, Chou YH, Blaivas M. Point of care ultrasound: a WFUMB position paper. Ultrasound Med Biol. 2017; 43:49–58. [PubMed: 27472989]

Fagenholz PJ, Gutman JA, Murray AF, Noble VE, Thomas SH, Harris NS. Chest ultrasonography for the diagnosis and monitoring of high-altitude pulmonary edema. Chest. 2007; 131:1013–1018. [PubMed: 17426204]

Frizzell LA, Zachary JF, O'Brien WD Jr. Effect of pulse polarity and energy on ultrasound-induced lung hemorrhage in adult rats. J Acoust Soc Am. 2003; 113:2912–2918. [PubMed: 12765408]

Gargani L, Volpicelli G. How I do it: lung ultrasound. Cardiovasc Ultrasound. 2014; 12:25. [PubMed: 24993976]

Hall MK, Hall J, Gross CP, Harish NJ, Liu R, Maroongroge S, Moore CL, Raio CC, Taylor RA. Use of Point-of-Care Ultrasound in the Emergency Department: Insights From the 2012 Medicare National Payment Data Set. J Ultrasound Med. 2016; 35:2467–2474. [PubMed: 27698180]

Irwin Z, Cook JO. Advances in Point-of-Care Thoracic Ultrasound. Emerg Med Clin North Am. 2016; 34:151–157. [PubMed: 26614246]

Joyner CR Jr, Herman RJ, Reid JM. Reflected ultrasound in the detection and localization of pleural effusion. JAMA. 1967; 200:399–402. [PubMed: 6071511]

Lichtenstein DA, Menu Y. A bedside ultrasound sign ruling out pneumothorax in the critically ill. Lung sliding. Chest. 1995; 108:1345–1348. [PubMed: 7587439]

Lichtenstein D. Lung ultrasound in the critically ill. Curr Opin Crit Care. 2014; 20:315–322. [PubMed: 24758984]

Lichtenstein DA. BLUE-protocol and FALLS-protocol: two applications of lung ultrasound in the critically ill. Chest. 2015; 147:1659–1670. [PubMed: 26033127]

Liu J, Liu F, Liu Y, Wang HW, Feng ZC. Lung ultrasonography for the diagnosis of severe neonatal pneumonia. Chest. 2014; 146:383–388. [PubMed: 24833216]

Lumb, P., Karakitsos, D., editors. Critical Care Ultrasound. Philadelphia: Elsevier; 2015. Section VI General Chest Ultrasound; p. 105-137.

Miller LD, Joyner CR Jr, Dudrick SJ, Eskin DJ. Clinical use of ultrasound in the early diagnosis of pulmonary embolism. Ann Surg. 1967; 166:381–393. [PubMed: 6039597]

Miller DL. Induction of pulmonary hemorrhage in rats during diagnostic ultrasound. Ultrasound Med Biol. 2012; 38:1476–1482. [PubMed: 22698500]

Miller DL. Mechanisms for induction of pulmonary capillary hemorrhage by diagnostic ultrasound: review and consideration of acoustical radiation surface pressure. Ultrasound Med Biol. 2016; 42:2743–2757. [PubMed: 27649878]

Miller DL, Dou C, Raghavendran K. Pulmonary capillary hemorrhage induced by fixed-beam pulsed ultrasound. Ultrasound Med Biol. 2015a; 41:2212–9. [PubMed: 25933710]

Miller DL, Dou C, Raghavendran K. The dependence of thresholds for pulmonary capillary hemorrhage on diagnostic ultrasound frequency. Ultrasound Med Biol. 2015b; 41:1640–1650. [PubMed: 25746909]

Miller DL, Dou C, Raghavendran K. Anesthetic techniques influence the induction of pulmonary capillary hemorrhage during diagnostic ultrasound in rats. J Ultras Med. 2015c; 34:289–297.

Miller DL, Dou C, Dong Z, Raghavendran K. The influence of dexmedetomidine on ultrasound-induced pulmonary capillary hemorrhage in rats. Ultrasound Med Biol. 2016a; 42:964–970. [PubMed: 26774471]

Miller DL, Dong Z, Dou C, Raghavendran K. Influence of scan duration on pulmonary capillary hemorrhage induced by diagnostic ultrasound. Ultrasound Med Biol. 2016b; 42:1942–1950. [PubMed: 27117631]

O'Brien WD Jr, Simpson DG, Ho MH, Miller RJ, Frizzell LA, Zachary JF. Superthreshold behavior and threshold estimation of ultrasound-induced lung hemorrhage in pigs: role of age dependency. IEEE Trans Ultrason Ferroelectr Freq Control. 2003a; 50:153–169. [PubMed: 12625588]

O'Brien WD, Simpson DG, Frizzell LA, Zachary JF. Threshold estimates and superthreshold behavior of ultrasound-induced lung hemorrhage in adult rats: role of pulse duration. Ultrasound Med Biol. 2003b; 29:1625–1634. [PubMed: 14654157]

Pereda MA, Chavez MA, Hooper-Miele CC, Gilman RH, Steinhoff MC, Ellington LE, Gross M, Price C, Tielsch JM6, Checkley W7. Lung ultrasound for the diagnosis of pneumonia in children: a meta-analysis. Pediatrics. 2015; 135:714–722. [PubMed: 25780071]

Sartori S, Tombesi P. Emerging roles for transthoracic ultrasonography in pleuropulmonary pathology. World J Radiol. 2010; 2:83–90. [PubMed: 21160921]

Sekiguchi H. Tools of the Trade: Point-of-Care Ultrasonography as a Stethoscope. Semin Respir Crit Care Med. 2016; 37:68–87. [PubMed: 26844609]

Sferrazza Papa GF, Mondoni M, Volpicelli G, Carlucci P, Di Marco F, Parazzini EM, Reali F, Pellegrino GM, Fracasso P, Sferrazza Papa S, Colombo L, Centanni S. Point-of-Care Lung Sonography: An Audit of 1150 Examinations. J Ultrasound Med. 2017; 36:1687–1692. [PubMed: 28417478]

Vargas PE, Lopez-Candales A. Essential echocardiographic evaluation in patients with suspected pulmonary hypertension: an overview for the practicing physician. Postgrad Med. 2016; 128:208–22. [PubMed: 26560900]

Volpicelli G. Lung sonography. J Ultrasound Med. 2013; 32:165–171. [PubMed: 23269722]

Weitzel WF, Hamilton J, Wang X, Bull JL, Vollmer A, Bowman A, Rubin J, Kruger GH, Gao J, Heung M, Rao P. Quantitative lung ultrasound comet measurement: method and initial clinical results. Blood Purif. 2015; 39:37–44. [PubMed: 25660686]

Zachary JF, Sempsrott JM, Frizzell LA, Simpson DG, O'Brien WD Jr. Superthreshold behavior and threshold estimation of ultrasound-induced lung hemorrhage in adult mice and rats. IEEE Trans Ultrason Ferroelectr Freq Control. 2001; 48:581–592. [PubMed: 11370372]

Zoccali C, Torino C, Tripepi R, Tripepi G, D'Arrigo G, Postorino M, Gargani L, Sicari R, Picano E, Mallamaci F. Lung US in CKD Working Group. Pulmonary congestion predicts cardiac events and mortality in ESRD. J Am Soc Nephrol. 2013; 24:639–646. [PubMed: 23449536]

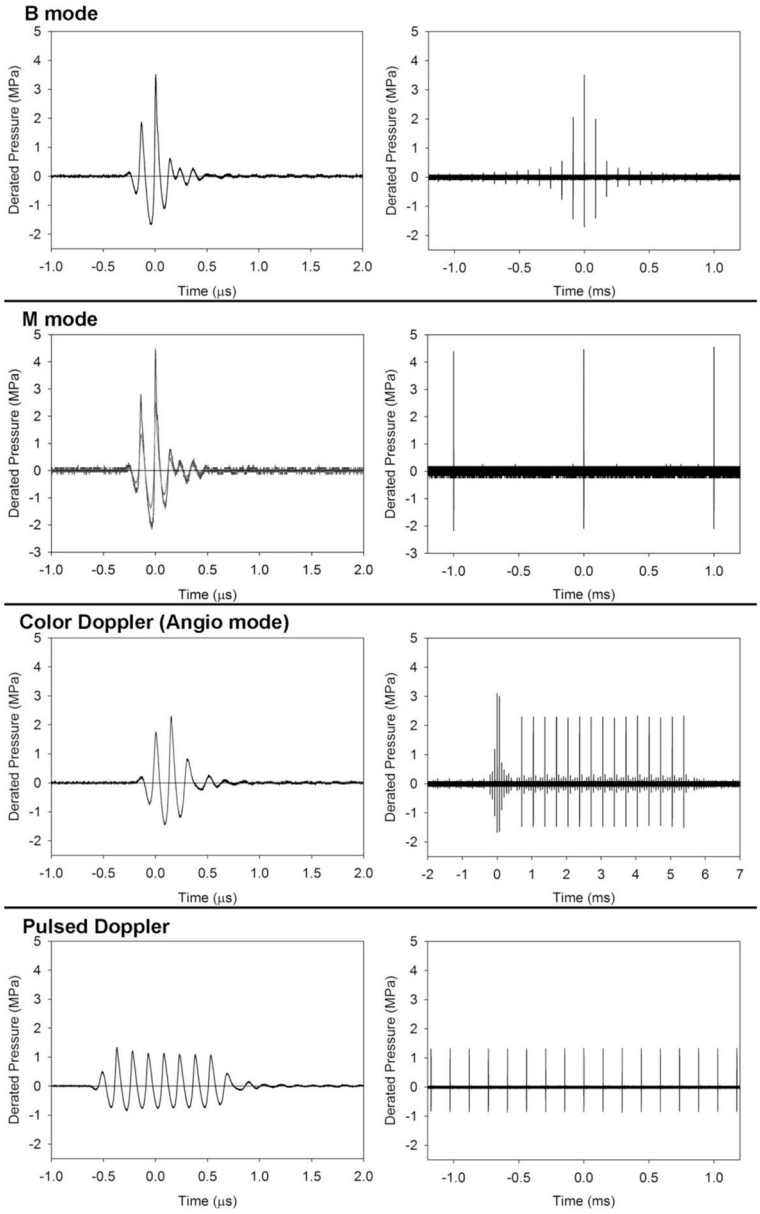

Figure 1.

A display of the pulse waveforms for each of the diagnostic ultrasound modes used. The power levels were the lowest settings with statistically significant pulmonary capillary hemorrhage. For B and Angio Doppler imaging modes, the pulses are short (left column) and several pulses appear in the sequence as the scanning beam passes by the hydrophone (right column). For B mode, this produces a rapid rise and fall of amplitudes. For the Angio Doppler mode, there is a brief B-mode sequence, for the greyscale background image, and sequences of 15 pulses which accurately determine the motion (normally blood flow). This sequence also passes by the hydrophone with rising and falling amplitudes; here only the maximum sequence is shown at the center of the Doppler box. For the fixed beam pulsed modes, the sequence (right column) is simply a pulse train at the pulse repetition period. The

M mode pulse (left column) is the same for both the 15 s and 5 min exposures. The pulsed-Doppler pulse is relatively long to yield accurate velocity measurements within the sample volume.

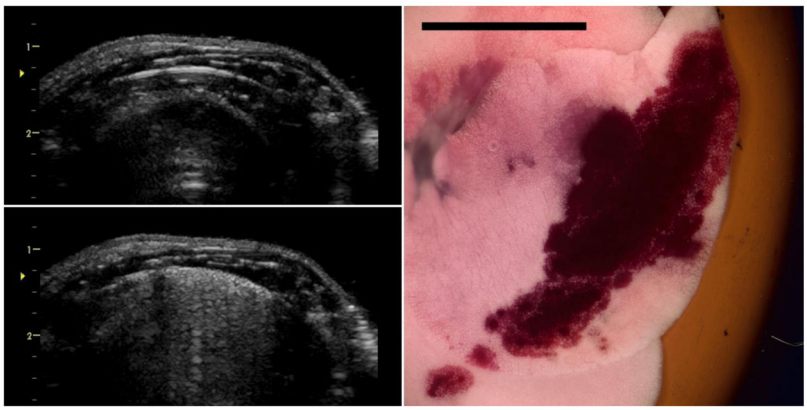

Figure 2.

Images for the B mode exposure at 0 dB (maximum power). The initial image (upper left) shows the bright-line lung reflection at 1.3 cm depth (approximately at the focus arrowhead). After 5 min the image (lower left) shows the resulting comet tail artifacts extending across the surface (sometimes called the “white lung” sign) due to the pulmonary capillary hemorrhage. The right image shows the right medial lung lobe with a hemorrhage area corresponding to the ultrasound scan plane. Scale bar 1 cm.

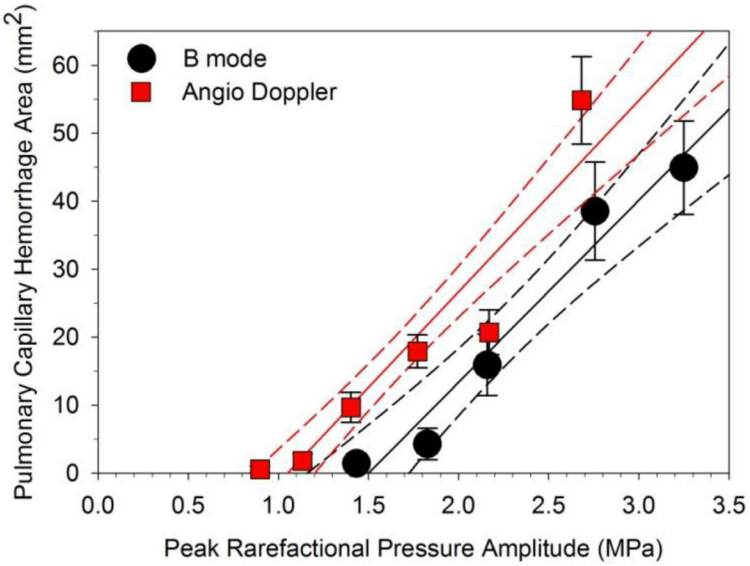

Figure 3.

A plot of the pulmonary capillary hemorrhage area measurements for B mode (black circles) and Angio Doppler mode (red squares) for the PRPAs used. A linear regression is shown for each plot (lines) with 95% confidence intervals (dashed lines). Each point is the mean for six rats with standard error bars. Both trends are increasing area above a threshold.

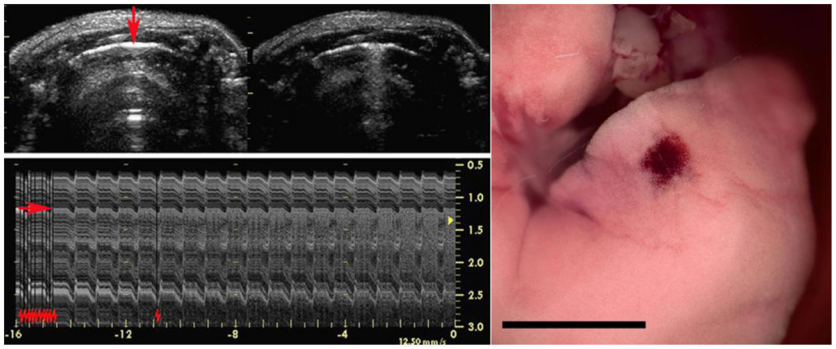

Figure 4.

Images for the M mode 15 s exposure at 0 dB (maximum power). The initial image (upper left on the left) shows the bright-line lung reflection at 1.3 cm with the M mode aim indicated by the red arrow. After 5 min the image (upper left on the right) shows the resulting comet tail artifacts extending across a small region of the surface where the fixed beam was aimed. The lower left image shows the M mode trace proceeding from left to right for 16 s: the red arrow indicates the lung surface, while the repeated red hash marks indicate the increase in power steps from −20 dB to 0 dB (stepped back down immediately after the trace was recorded). Note that the trace shows a progressive breakup as the comet tail artifact forms along the beam line. The lung image of the medial lobe has a hemorrhage spot corresponding to the beam aim point. Scale bar 1 cm.

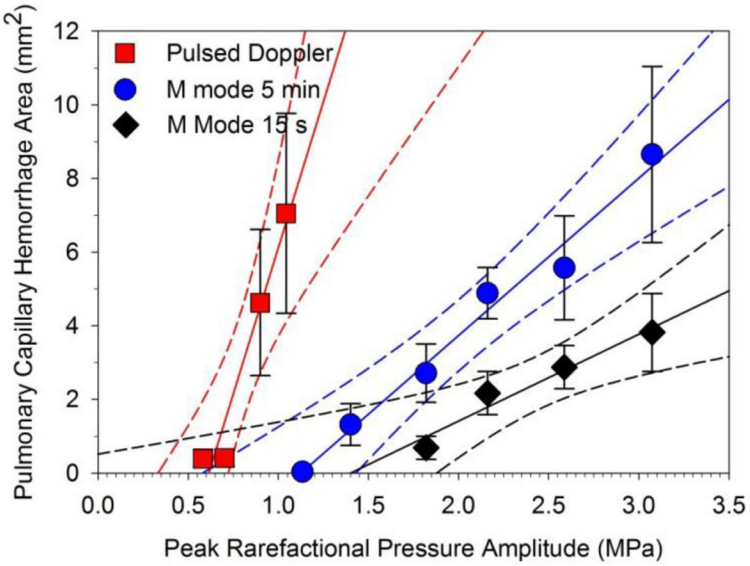

Figure 5.

A plot of the pulmonary capillary hemorrhage area measurements for M mode for 5 min (blue circles) and 15 s (black diamonds) and pulsed Doppler mode (red squares) for the PRPAs. Linear regressions are shown for each plot (lines), with 95% confidence intervals (dashed lines). Each point is the mean for six rats with standard error bars. Both M mode trends are increasing area above a threshold. The pulse Doppler mode is much more effective at the relatively low PRPA values.

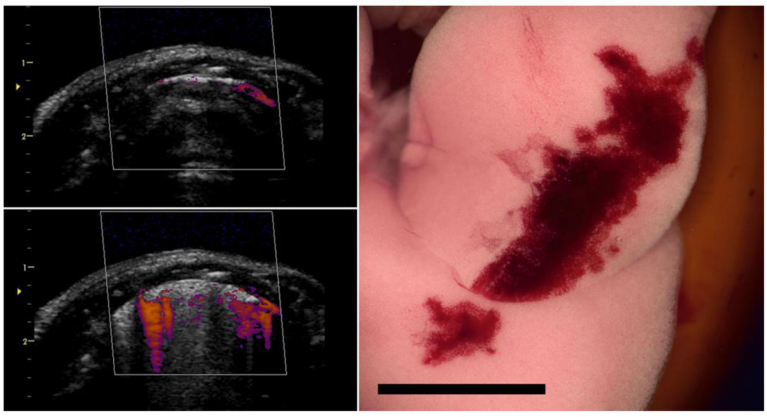

Figure 6.

Images for the Angio Doppler mode exposure at 0 dB (maximum power) as for the B mode (Fig. 2). In this case the images (upper and lower left) show the Angio color display as well as the background grey scale (B mode) image. The hemorrhage area on the lung is similar to the B mode effect. Scale bar 1 cm.

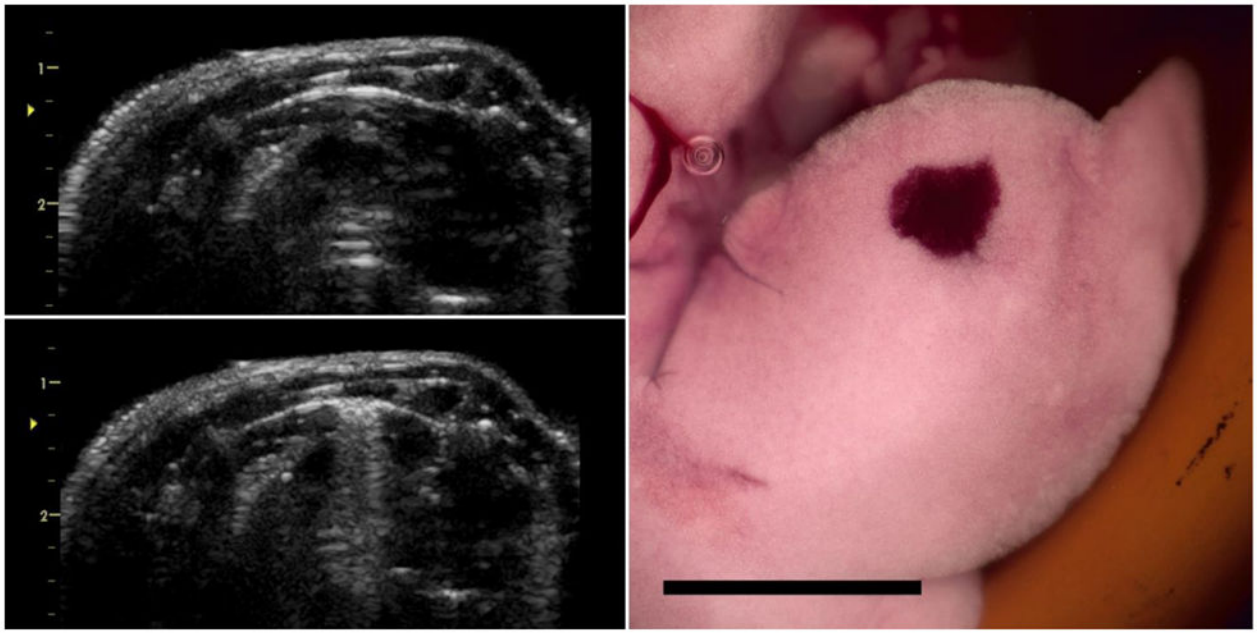

Figure 7.

Images for the pulsed Doppler mode exposure at 0 dB (maximum power), presented as for the Angio Doppler mode. The initial B mode image (upper left) shows the bright-line lung reflection, followed by the narrow comet tail artifact display (lower left) after 5 min. The right medial lung lobe (right) has the characteristic hemorrhage spot corresponding to the pulsed Doppler aim point. Scale bar 1 cm.

Table 1

The pulsing parameters used for the 4 exposure modes, all with an observed frequency of 6.6 MHz. The Doppler mode sample volumes were 0.4 mm for Angio mode and 1 mm for pulsed Doppler. Thresholds are given for the PRPA, PMPA, I_{SPPA} and in situ MI based on linear regression of PCH area versus PRPA as shown in Figs. 3 and 5.

Mode Condition	Pulse ns	PRP μs	fps Hz	PRPA MPa	r^2	PMPA MPa	I_{SPPA} W cm^{-2}	MI_{IS} MPa MHz$^{-½}$
B	268	96	60	1.5	0.69	2.2	87	0.58
M 15s	269	1000		1.4	0.45	2.1	85	0.54
M 5 m	269	1000	-	1.1	0.51	1.6	50	0.44
Angio D	319	335	17.5	1.1	0.76	1.3	42	0.41
Pulsed D	1130	147	-	0.6	0.35	0.7	12	0.24

Pulse, pulse duration observed at −6 dB power setting; PRP, pulse repetition period; fps frames per second; D Doppler mode; PRPA, peak rarefactional pressure amplitude in situ; PMPA, pulse mean pressure amplitude in situ; I_{SPPA}, spatial peak pulse average intensity in situ; MI, Mechanical Index in situ calculated as in situ PRPA (MPa)x(6.6 MHz)$^{-½}$.

Table 2

Pulmonary Capillary hemorrhage results for each of the groups (mean with standard deviation) for the different modes having the given exposure parameters of pressure amplitude and intensity. The sham utilized the B mode imaging used for aiming.

Protocol	PRPA MPa	I_{SPPA} W/cm^2	Positive Proportion	Comets %	Area mm^2	Volume mm^3	Depth mm	A vs sham p
B	3.3	468	6/6	89±11	45±17	90±61	2.0±1.0	0.002
mode	2.8	326	6/6	82±10	39±18	56±45	1.5±0.5	0.002
5 min	2.2	203	6/6	69±17	16±11	13±11	0.82±0.40	0.002
	1.8	129	5/6	24±18	4.3±5.6	3.1±4.3	0.52±0.30	0.015
	1.4	78	3/6	7.9±12.4	1.4±2.1	0.9±1.4	0.21±0.34	0.18
M	3.1	438	7/7	15.7±4.8	3.8±2.8	7.8±8.9	1.6±0.9	0.001
mode	2.6	321	6/6	14.1±4.3	2.9±1.4	4.2±2.5	1.4±1.0	0.002
15 s	2.2	214	6/6	13.1±4.5	2.2±1.4	2.6±2.0	1.12±0.30	0.002
	1.8	138	3/6	5.4±6.0	0.7±.0.8	0.5±0.6	0.38±0.46	0.18
M	3.1	438	6/6	28±16	8.7±5.9	18.6±17.4	2.3±0.5	0.002
mode	2.6	321	6/6	21±7	5.6±3.5	8.8±6.3	1.4±0.6	0.002
5 min	2.2	214	6/6	22±4	4.9±1.7	6.8±3.3	1.3±0.3	0.002
	1.8	138	5/6	13.4±7.5	2.7±1.9	2.8±2.2	0.81±0.45	0.015
	1.4	85	5/6	10.7±5.3	1.3±1.4	1.0±1.3	0.62±0.38	0.015
	1.1	50	1/6	2.2±5.3	0.04±0.09	0±0	0±0	0.70
Angio	2.7	375	6/6	87±7.5	55±16	99±39	2.1±0.4	0.002
Doppler	2.2	202	6/6	85±14	21±8	24±16	1.3±0.4	0.002
5 min	1.8	144	6/6	77±14	18±6	23±12	1.2±0.3	0.002
	1.4	85	6/6	50±19	9.7±5.4	8.6±6.3	0.98±0.35	0.002
	1.1	51	4/6	14.8±16.7	1.8±2.6	1.2±1.9	0.36±0.42	0.18
	0.9	30	2/6	5.5±10.2	0.6±1.2	0.3±0.6	0.12±0.29	0.39
Pulsed	1.0	44	6/6	20.3±7.8	7.1±6.6	9.1±11.2	1.2±0.4	0.002
Doppler	0.9	27	6/6	27.9±23.2	4.6±4.9	4.9±6.9	1.1±0.6	0.002
5 min	0.7	17	3/8	4.7±6.6	0.4±0.6	0.2±0.4	0.15±0.28	0.28
	0.6	10	2/6	5.2±8.1	0.4±0.6	0.2±0.4	0.19±0.29	0.39

Protocol	PRPA MPa	I_{SPPA} W/cm^2	Positive Proportion	Comets %	Area mm^2	Volume mm^3	Depth mm	A vs sham p
Sham	0.4	3.8	0/6	0.0	0.0	0.0	0.0	-

A vs. sham is a Mann-Whitney rank sum test of PCH areas relative to the sham.